lubricants

MDPI

Article

A Numerical Model for the Analysis of the Bearings of a Diesel Engine Subjected to Conditions of Wear and Misalignment

Carlos Pardo García [1], Jhan Piero Rojas [2] and Sofia Orjuela Abril [3,*]

[1] Programa de Ingeniería de Sistemas, Universidad Francisco de Paula Santander, Avenida Gran Colombia No. 12E-96 Barrio Colsag, San José de Cúcuta 540001, Colombia; carlospardo@ufps.edu.co
[2] Facultad de Ingeniería, Universidad Francisco de Paula Santander, Avenida Gran Colombia No. 12E-96 Barrio Colsag, San José de Cúcuta 540001, Colombia; jhanpierorojas@ufps.edu.co
[3] Programa de Administración de Empresas, Universidad Francisco de Paula Santander, Avenida Gran Colombia No. 12E-96 Barrio Colsag, San José de Cúcuta 540001, Colombia
* Correspondence: sofiaorjuela@ufps.edu.co; Tel.: +577-569-00-88

Abstract: In the present work, a numerical model is developed to investigate the influence of wear and misalignment on the bearings of a stationary diesel engine. The model implemented considers the effects of surface wear on the bearing, cavitation effects, and surface roughness. For the numerical analysis, changes in the surface roughness of $\sigma = 0.75$ µm, $\sigma = 1$ µm, and $\sigma = 1.25$ µm are defined, and changes in the bearing load of 50%, 75%, and 100%. The results demonstrated that increasing the surface roughness intensifies the bearing wear, which represents 18% and 140% of the bearing clearance for the roughness of $\sigma = 1$ µm and $\sigma = 1.25$ µm, respectively. Additionally, the surface roughness causes a considerable increase in the bearing wear rate. The results described a maximum wear rate of 20 µm/s. In general, increasing the bearing load by 25% doubles the hydrodynamic pressure conditions increases friction force by 33%, and reduces lubrication film thickness by 12%. The analysis of the angle of deflection, ϕ_x and ϕ_y, shows that the moment and the degree of misalignment tend to increase significantly with the increase in the magnitude of the angle ϕ_y. Negative angles of deflection, ϕ_x, produce a greater increase in the degree of misalignment and the moment. This implies a greater chance of contact with the bearing surface. In conclusion, the proposed methodology serves as a reliable tool to simultaneously evaluate key parameters on the tribological behavior of bearings that further extend their endurance and minimize wear damage.

Keywords: engine bearings; deflection angle; misalignment; surface roughness

Citation: Pardo García, C.; Rojas, J.P.; Orjuela Abril, S. A Numerical Model for the Analysis of the Bearings of a Diesel Engine Subjected to Conditions of Wear and Misalignment. *Lubricants* **2021**, *9*, 42. https://doi.org/10.3390/lubricants9040042

Received: 16 March 2021
Accepted: 6 April 2021
Published: 9 April 2021

1. Introduction

The necessity to propose concrete innovations in engine operation has become essential in the short-midterm status of these thermal machines. Nowadays, internal combustion engines (ICE) play a predominant role in numerous applications, but the inherent energy losses and global emissions have paved the way for the consolidation of different strategies to establish a more reliable and eco-friendly operation [1–3]. Particularly, energy losses overcome a great share of the global energy losses that both increase fuel consumption and limit overall efficiency. Therefore, different proposals have been successfully established, such as control strategies, compression ring sealing capacity, hydroxy doping, biofuels, and cylinder bore coatings materials, among others [4,5]. Particularly in mechanical power losses, bearings experience a distinguishing contribution in ICEs, since they enable the transmission of forces and relative movement. They are designed to operate under hydrodynamic regime conditions, thus enabling the separation between the contact surfaces is guaranteed. However, this condition cannot always be maintained throughout the life of the bearing. Therefore, limited and mixed lubrication regimes may occur. These regimes imply the coexistence of hydrodynamic contact pressure and roughness, causing greater friction losses, increasing the probability of failure and wear. The consideration of a

perfectly aligned bearing is an approximation that is difficult to achieve in real conditions. This can be due to multiple factors ranging from imperfections in the manufacturing process to installation errors. If the axes and bushing axes are not kept parallel, the protective lubrication film in one area will weaken, producing a risk of surface-to-surface contact [6,7]. Thus, the wear prediction based on numerical methodologies has gradually gained attention as a robust tool to improve the bearing design and further extend the service time [4].

Bearings typically experience misalignment, causing uneven wear processes and catastrophic failures. In the particular case of motor bearings, they are susceptible to misalignment, which induces a reduction in performance and component life [8,9]. Additionally, misalignment causes a reduction in the lubrication film, resulting in an increase in eccentricity. This increases the possibility of direct metal-to-metal contact [10]. Wear caused by misalignment is reflected in bearing dynamic performance, noise levels, increased coefficient of friction, vibration levels, and reduction in load capacity [11,12]. The analysis of this type of component is complex due to the condition of non-stationary movement that changes significantly in the face of variations in magnitude and direction. Due to the negative effects mentioned above, it is necessary to carry out research for the evaluation of bearing wear [5,13–15].

Several investigations have focused on wear contact surfaces based on quantitative and qualitative approaches. Nabhan et al. [16] evaluated the wear rate in Babbitt-type sliding bearings by experimental methods. In the study, the parameters of load, speed, friction coefficient, and temperature were considered. The results indicated that bearing speed and load are the main factors contributing to wear. Aghdam and Khonsari [17] used an energy-based approach to analyze and predict wear in grease-lubricated spherical bearings. Chun and Khonsari [18] established a theoretical method to predict wear in bearings exposed to a mixed elastohydrodynamic lubrication regime. The method used is based on a roughness contact model to take into account the effects of elastohydrodynamic lubrication (EHL). Sander et al. [19] used the Archard wear equation and the Greenwood and Tripp contact model to investigate wear in trunnion bearing bearings. Springis et al. [16] proposed a numerical model based on fatigue theory to calculate wear. The model considers the microtopography and the surface roughness parameters. Jia et al. [20] established a fatigue wear model based on micropitting to simulate wear in the bearing surface contact under EHL conditions.

Additionally, in recent years, the effect of misalignment on lubrication characteristics has been studied. Gu et al. [21] investigated the hydrodynamic properties in the presence of misalignment and different types of textures. The results show that the increase in the deflection angles causes a reduction in the tribological performance of the bearing. Li et al. [22] evaluated the effect of misalignment on the dynamic conditions of gas bearings. The conclusions show that the presence of misalignment has a significant influence on the dynamic coefficients. In another investigation, Li et al. [23] studied the thermo-hydrodynamic lubrication in support bearings with the presence of misalignment considering axial movement. The results indicate that misalignment affects the lubrication characteristics more clearly when there is a low-speed condition, higher eccentricities, and angle of inclination. Zhu et al. [24] considered the lubrication conditions of rough surface bearings with misalignment. Research shows that roughness increases the effect of misalignment. Feng et al. [25] evaluated the static and dynamic characteristics of water-lubricated bearings, taking into account turbulent and misalignment effects. The results show that turbulence improves load capacity. Zheng et al. [26] investigated the influence of viscosity and oil film thickness on the performance of misaligned slide bearings. Xie et al. [27] studied the performance of water lubrication and dynamic characteristics in bearings with misalignment using CFD. In addition, the different lubrication regimes were evaluated, such as limit, mixed, and hydrodynamic lubrication [28–32].

In this article, a numerical model is built for the study of the bearings of a stationary diesel engine. For the development of the model, the phenomenon of cavitation and the

effects of surface roughness are considered together, which are not generally analyzed in a compound methodology in former research. Thus, this work establishes a further effort to shorten the knowledge gap involved in the characterization of the tribological performance of engine bearings. In this sense, the proposed methodology simultaneously evaluates the influence of surface roughness, load conditions, angle of deflection, wear, and performance parameters of the bearing performance. The objective of the research is to make a contribution through the development of a numerical model that allows for estimating the wear in the bearings of a modern diesel engine, taking into consideration factors such as surface asperity, cavitation effects, and misalignment conditions, which are generally analyzed individually in the literature. In what follows: Section 2 depicts the main features of the numerical model and constitutive formulation. Next, Section 3 outlines the numerical procedure followed in the investigation and displays the validation results. Section 4 introduces the core findings of this work and actively discusses the findings. Finally, Section 5 sets the concluding remarks, limitations, and future endeavors in this field.

2. Materials and Methods

This section aims to describe the equations required for the construction of the numerical model used in the present study. The lubrication film thickness, Reynolds equation, dynamic forces on the bearing, and bearing wear model will be studied in order to analyze the bearings of a diesel engine subjected to conditions of wear and misalignment.

2.1. Lubrication Film Thickness

First, Figure 1 describes the main characteristics and geometric position of a bearing with the presence of misalignment in the engine.

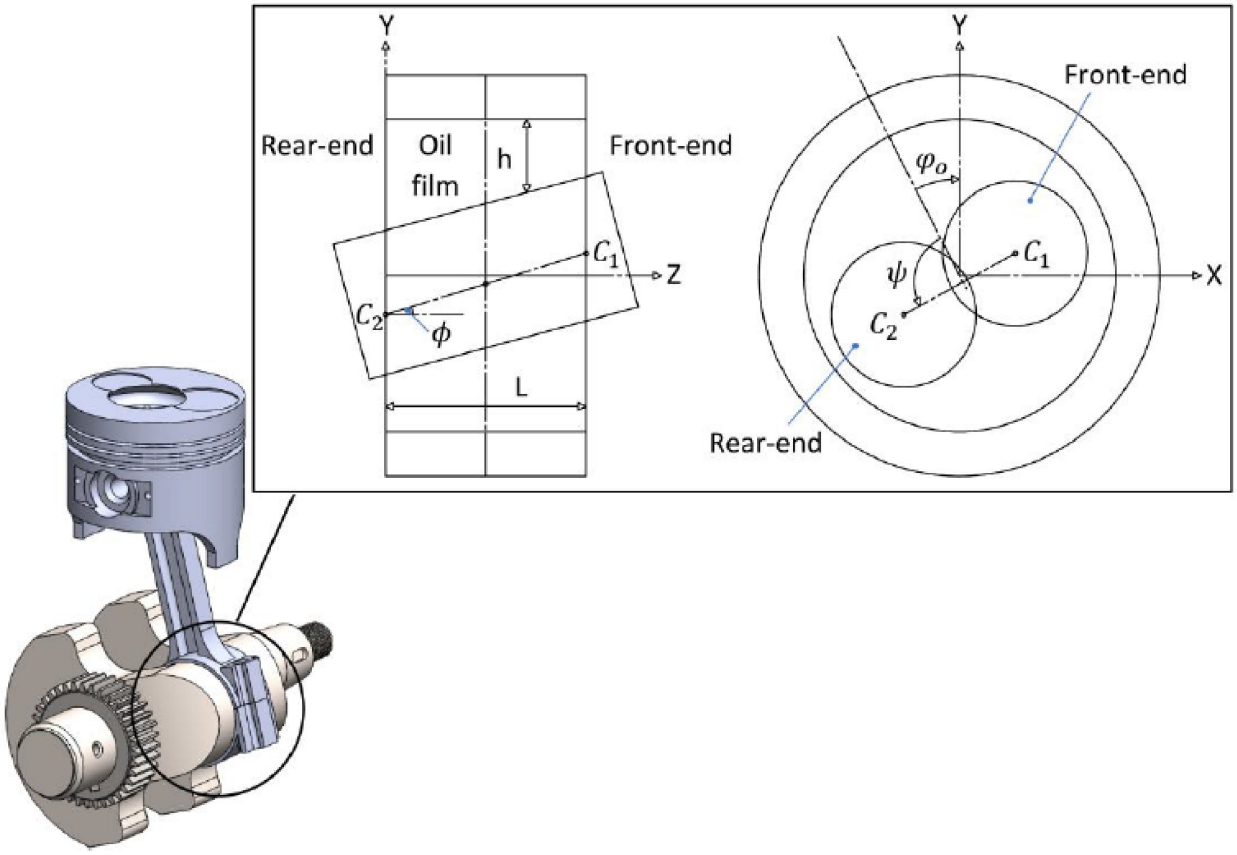

Figure 1. Configuration of a bearing with misalignment.

The thickness of the lubrication film on the bearing with the presence of wear and misalignment is described by Equation (1) [33].

$$h = e_o \cdot \cos(\phi - \varphi_o) + e' \cdot \cos(\phi - \psi - \varphi_o) \cdot \left(\frac{z}{L} - 0.5\right) + C + \delta \quad (1)$$

where ϕ is the angular position of the bearing, ψ is the misalignment angle, φ_o the attitude angle between the line of centers and the Y-axis, e_o is the eccentricity in the mid-plane of the bearing, e' is the length of the projection of the misaligned journal on the mid-plane (if the bearing is not misaligned, $e' = 0$), L is the length of the bearing, C is the bearing radial clearance, and δ is the depth of wear.

The thickness of the dimensionless lubrication film $\left(\overline{h}\right)$ is calculated using Equation (2).

$$\overline{h} = \varepsilon_o \cdot \cos(\phi - \varphi_o) + \varepsilon' \cdot \cos(\phi - \psi - \varphi_o) \cdot (\overline{z} - 0.5) + 1 + \overline{\delta} \quad (2)$$

where $\overline{h}$, ε_o, $\overline{z}$, and $\overline{\delta}$ are dimensionless parameters defined by Equations (3)–(6).

$$\overline{h} = \frac{h}{C} \quad (3)$$

$$\varepsilon_o = \frac{e_0}{C} \quad (4)$$

$$\overline{z} = \frac{z}{L} \quad (5)$$

$$\overline{\delta} = \frac{\delta}{C} \quad (6)$$

The parameter ε' is the misalignment eccentricity ratio defined as $\varepsilon' = \varepsilon'_{max} \cdot A_m$, where A_m is the degree of the misalignment. The term ε'_{max} is calculated from Equation (7) [34].

$$\varepsilon'_{max} = 2 \cdot \sqrt{1 - \varepsilon_0^2 \cdot (\sin\psi)^2} - \varepsilon_0 \cdot |\cos\psi| \quad (7)$$

To determine the deflection of the journal in the horizontal and vertical direction, the angles ϕ_x and ϕ_y are used. The relationship between the deflection angles (ϕ_x, ϕ_y) and the misalignment angle (ψ) is shown in Equations (8) and (9).

$$\psi = \tan^{-1}\left(-\frac{\tan\phi_x}{\tan\phi_y}\right) - \varphi_o, \ \phi_y < 0 \quad (8)$$

$$\psi = \tan^{-1}\left(-\frac{\tan\phi_x}{\tan\phi_y}\right) - \varphi_o + \pi, \ \phi_y > 0 \quad (9)$$

2.2. Reynolds Equation

The Reynolds equation that is normally used to define the lubrication film pressure distribution is shown in Equation (10).

$$\frac{\partial}{\partial x}\left(\rho \cdot F_2 \cdot \frac{\partial P}{\partial x}\right) + \frac{\partial}{\partial z}\left(\rho \cdot F_2 \cdot \frac{\partial P}{\partial z}\right) = \frac{\partial}{\partial x}\left(\rho \cdot u_s \cdot \left[h - \frac{F_1}{F_0}\right]\right) + \frac{\partial}{\partial t}(\rho h) \quad (10)$$

where F_i $(i = 0, 1, 2)$ are viscosity functions, which are determined from the following equations:

$$F_0 = \int_0^h \frac{dy}{\eta} \quad (11)$$

$$F_1 = \int_0^h y \frac{dy}{\eta} \quad (12)$$

$$F_2 = \int_0^h \frac{1}{\eta} \cdot \left(y^2 - y \frac{F_1}{F_0} \right) dy \tag{13}$$

where η is the viscosity of the lubricant. To consider the effects of cavitation, the modified Reynolds equation proposed by Elrod and Adams [35] is used as expressed in Equation (14).

$$\frac{\partial}{\partial x}\left(g(\Theta) \cdot \beta \cdot F_2 \cdot \frac{\partial \Theta}{\partial x} \right) + \frac{\partial}{\partial z}\left(g(\Theta) \cdot \beta \cdot F_2 \cdot \frac{\partial \Theta}{\partial z} \right) = \frac{\partial}{\partial x}\left(u_s \cdot \Theta \cdot \left[h - \frac{F_1}{F_0} \right] \right) + \frac{\partial}{\partial t}(\Theta \cdot \mathrm{h}) \tag{14}$$

where β is the bulk modulus of the lubricant and u_s is the shaft speed. The new parameter Θ in the Reynolds equation is known as the fractional film content, and it is defined as shown in Equation (15).

$$\Theta = \frac{\rho}{\rho_c} \tag{15}$$

where ρ_c is the density of the lubricant under cavitation pressure conditions. $g(\Theta)$ is a binary parameter defined as:

$$g(\Theta) = 1, \quad \Theta \geq 1 \tag{16}$$

$$g(\Theta) = 0, \quad \Theta < 1 \tag{17}$$

The dimensionless form of the Elrod and Adams [35] equation is shown below:

$$\frac{\partial}{\partial \phi}\left(\overline{h}^3 \cdot \overline{F}_2 \cdot \frac{\partial \overline{P}}{\partial \theta} \right) + \frac{1}{4A_r^2} \cdot \frac{\partial}{\partial \overline{z}}\left(\overline{h}^3 \cdot \overline{F}_2 \cdot \frac{\partial \overline{P}}{\partial \overline{z}} \right) = \frac{\partial}{\partial \phi}\left(\overline{U} \cdot \Theta \cdot \overline{h} \right) + \frac{\partial}{\partial \overline{t}}\left(\Theta \cdot \overline{h} \right) \tag{18}$$

where $\overline{U}$ and A_r are the dimensionless speed and the aspect ratio defined by Equations (19) and (20).

$$\overline{U} = 1 - \frac{\overline{F}_1}{\overline{h} \cdot \overline{F}_0} \tag{19}$$

$$A_r = \frac{L}{2R} \tag{20}$$

where R is the journal radius. The dimensionless viscosity functions ($\overline{F}_0$, $\overline{F}_1$ and $\overline{F}_2$) are defined as:

$$\overline{F}_0 = \int_0^1 \frac{d\overline{y}}{\overline{\eta}} \tag{21}$$

$$\overline{F}_1 = \int_0^1 \frac{\overline{y}}{\overline{\eta}} d\overline{y} \tag{22}$$

$$\overline{F}_2 = \int_0^1 \left[\frac{1}{\overline{\eta}} \cdot \left(\overline{y}^2 - \overline{y} \frac{\overline{F}_1}{\overline{F}_0} \right) \right] d\overline{y} \tag{23}$$

For the numerical model, the discretized form of the Reynolds equation is used, which is composed of the Equations (24) and (25).

$$\begin{aligned} \frac{\left(\overline{U}\Theta\overline{h}\right)_{i,k}^n - \left(\overline{U}\Theta\overline{h}\right)_{i-1,k}^n}{\Delta\theta} &+ \frac{\left(\Theta\overline{h}\right)_{i,k}^n - \left(\Theta\overline{h}\right)_{i,k}^{n-1}}{\Delta\overline{t}} \\ &= \overline{P}_{i-1,k}^n \left[\frac{S_{i-1/2,k}^n}{(\Delta\theta)^2} \right] - \overline{P}_{i,j}^n \left[\frac{S_{i+1/2,k}^n + S_{i-1/2,k}^n}{(\Delta\theta)^2} + \frac{\left(S_{i,k+1/2}^n + S_{i,k-1/2}^n\right)}{4A_r{}^2 \cdot (\Delta\overline{z})^2} \right] \\ &+ \overline{P}_{i+1,k}^n \left[\frac{S_{i+1/2,k}^n}{(\Delta\theta)^2} \right] + \overline{P}_{i,k-1}^n \left[\frac{S_{i,k-1/2}^n}{4A_r{}^2 \cdot (\Delta\overline{z})^2} \right] + \overline{P}_{i,k+1}^n \left[\frac{S_{i,k+1/2}^n}{4A_r{}^2 \cdot (\Delta\overline{z})^2} \right] \end{aligned} \tag{24}$$

$$\begin{aligned}\left(\Theta\overline{h}\right)_{i,k}^{n}\left[\frac{\overline{U}_{i,k}}{\Delta\overline{x}}+\frac{1}{\Delta\overline{t}}\right]^{n} &= \left(\Theta\overline{h}\right)_{i-1,k}^{n}\left[\frac{\overline{U}_{i-1,k}}{\Delta\overline{x}}\right]^{n}+\left[\frac{1}{\Delta\overline{t}}\right]\left(\Theta\overline{h}\right)_{i,k}^{n-1}+\overline{P}_{i-1,k}^{n}\left[\frac{S_{i-1/2,k}^{n}}{(\Delta\overline{x})^{2}}\right]\\ &+\overline{P}_{i+1,k}^{n}\left[\frac{S_{i+1/2,k}^{n}}{(\Delta\overline{x})^{2}}\right]+\overline{P}_{i,k-1}^{n}\left[\frac{S_{i,k-1/2}^{n}}{4A_r{}^{2}\cdot(\Delta\overline{z})^{2}}\right]+\overline{P}_{i,k+1}^{n}\left[\frac{S_{i,k+1/2}^{n}}{4A_r{}^{2}\cdot(\Delta\overline{z})^{2}}\right]\\ &-\overline{P}_{i,k}^{n}\left[\frac{S_{i+1/2,k}^{n}+S_{i-1/2,k}^{n}}{(\Delta\overline{x})^{2}}+\frac{S_{i,k+1/2}^{n}+S_{i,k-1/2}^{n}}{4A_r{}^{2}\cdot(\Delta\overline{z})^{2}}\right]\end{aligned} \quad (25)$$

where $n-1$ and n are the previous and current steps of time. The parameter S is calculated from the average of two adjacent nodes.

$$S_{i\pm1/2,k}=\frac{\overline{h}_{i\pm1,k}^{3}F_{2\ i\pm1,k}+\overline{h}_{i,k}^{3}F_{2\ i,k}}{2} \quad (26)$$

$$S_{i,k\pm1/2}=\frac{\overline{h}_{i,k\pm1}^{3}F_{2\ i,k\pm1}+\overline{h}_{i,k}^{3}F_{2\ i,k}}{2} \quad (27)$$

2.3. Dynamic Forces on the Bearing

The journal bearing dynamic force equations are shown in Equations (28) and (29).

$$F_x+F_x^{oil}=\frac{\dot{e}_x^{t}-\dot{e}_x^{t+\Delta t}}{\Delta t}\cdot M_j \quad (28)$$

$$F_y+F_y^{oil}=\frac{\dot{e}_y^{t}-\dot{e}_y^{t+\Delta t}}{\Delta t}\cdot M_j \quad (29)$$

where F_x and F_y are the forces applied in the x–y direction, M_j is the mass of the journal, and F_x^{oil} and F_y^{oil} are the reaction forces of the lubricating oil. The equations of motion are described by Equations (30) and (31).

$$e_x^{t}=e_x^{t-\Delta t}+\dot{e}_x^{t}\cdot\Delta t \quad (30)$$

$$e_y^{t}=e_y^{t-\Delta t}+\dot{e}_y^{t}\cdot\Delta t \quad (31)$$

The lubricating oil forces $\left(F_x^{oil},F_y^{oil}\right)$ and the components of the moments (M_x,M_y) are determined by the following equations:

$$F_x^{oil}=\frac{\eta\cdot\overline{U}\cdot L\cdot R^{2}}{C^{2}}\cdot\int_0^1\int_0^{2\pi}\overline{P}\cdot\sin\phi d\overline{x}d\overline{z} \quad (32)$$

$$F_y^{oil}=-\frac{\eta\cdot\overline{U}\cdot L\cdot R^{2}}{C^{2}}\cdot\int_0^1\int_0^{2\pi}\overline{P}\cdot\cos\phi d\overline{x}d\overline{z} \quad (33)$$

$$M_x=\frac{\eta\cdot u_s\cdot L^{2}\cdot R^{2}}{C^{2}}\cdot\int_0^1\int_0^{2\pi}\overline{P}\cdot(\overline{z}-0.5)\cos\phi d\overline{x}d\overline{z} \quad (34)$$

$$M_y=\frac{\eta\cdot u_s\cdot L^{2}\cdot R^{2}}{C^{2}}\cdot\int_0^1\int_0^{2\pi}\overline{P}\cdot(\overline{z}-0.5)\sin\phi d\overline{x}d\overline{z} \quad (35)$$

where $\overline{P}$ is the dimensionless hydrodynamic pressure, calculated by Equation (36). The total moment (M_t) is determined by the Equation (37).

$$\overline{P}=P\cdot\frac{C^{2}}{R\cdot\eta\cdot u_s} \quad (36)$$

$$M_t=\sqrt{M_x+M_y} \quad (37)$$

By unifying Equations (28)–(31), the dynamic force equations can be expressed as:

$$f_x = \overline{F}_x + \overline{F}_x^{oil} - \frac{\overline{M}_j \cdot \left(\dot{\bar{\varepsilon}}_x^{\bar{t}} - \dot{\bar{\varepsilon}}_x^{\bar{t}-\Delta\bar{t}} \right)}{\Delta\bar{t}} = 0 \tag{38}$$

$$f_y = \overline{F}_y + \overline{F}_y^{oil} - \frac{\overline{M}_j \cdot \left(\dot{\bar{\varepsilon}}_y^{\bar{t}} - \dot{\bar{\varepsilon}}_y^{\bar{t}-\Delta\bar{t}} \right)}{\Delta\bar{t}} = 0 \tag{39}$$

where $\overline{F}_x, \overline{F}_y$ are the dimensionless forces and $\overline{M}_j$ is the dimensionless mass, which is calculated from Equations (40) and (41).

$$\overline{M}_j = \frac{C^3 \cdot M_j \cdot u_s}{\eta \cdot L \cdot R^4} \tag{40}$$

$$\overline{F}_x = \frac{C^2 \cdot F_x}{\eta \cdot L \cdot u_s \cdot R^2}, \quad \overline{F}_y = \frac{C^2 \cdot F_y}{\eta \cdot L \cdot u_s \cdot R^2} \tag{41}$$

Equations (38) and (39) is solved iteratively by calculating the Jacobian matrix shown below:

$$\begin{bmatrix} \frac{\partial f_x}{\partial \dot{\bar{\varepsilon}}_x^{\bar{t}}} & \frac{\partial f_x}{\partial \dot{\bar{\varepsilon}}_y^{\bar{t}}} \\ \frac{\partial f_y}{\partial \dot{\bar{\varepsilon}}_x^{\bar{t}}} & \frac{\partial f_y}{\partial \dot{\bar{\varepsilon}}_y^{\bar{t}}} \end{bmatrix} \begin{bmatrix} \Delta \left(\dot{\bar{\varepsilon}}_x^{\bar{t}} \right)^i \\ \Delta \left(\dot{\bar{\varepsilon}}_y^{\bar{t}} \right)^i \end{bmatrix} = - \begin{bmatrix} f_x \left\{ \left(\dot{\bar{\varepsilon}}_x^{\bar{t}} \right)^i, \left(\dot{\bar{\varepsilon}}_y^{\bar{t}} \right)^i \right\} \\ f_y \left\{ \left(\dot{\bar{\varepsilon}}_x^{\bar{t}} \right)^i, \left(\dot{\bar{\varepsilon}}_y^{\bar{t}} \right)^i \right\} \end{bmatrix} \tag{42}$$

2.4. Bearing Wear Model

To determine the wear parameter δ (see Equation (1)), the model proposed by Archard [36] is implemented, which describes the wear due to roughness contact as shown in Equation (43).

$$\vartheta = \frac{c_k \cdot s_d \cdot W_l}{H} \tag{43}$$

where c_k is the wear coefficient $\left(c_k = 3.11 \times 10^{-16}\ \mathrm{Pa}^{-1} \right)$, ϑ is the wear volume, s_d is the sliding distance, H is the hardness, and W_l is the applied load. The wear rate is defined as:

$$\dot{\delta} = \frac{c_k \cdot \pi \cdot R \cdot N}{30 \cdot H} \cdot \frac{W_l}{A_n} \tag{44}$$

where N and A_n are the shaft speed in revolutions per minute and contact area, respectively.

2.5. Contact Model

To consider the effect of a rough surface, the Kogut and Etsion [37] contact model is used, which mainly considers the plasticity index (Φ), as shown in Equation (45).

$$\Phi = 2 \left(\frac{\sigma_s}{\beta_s} \right)^{1/2} \cdot \frac{E'}{\pi \cdot H \cdot K_c} \tag{45}$$

where E' is the Hertz elastic modulus, β_s is the asperity radius, and σ_s is the mean of asperity heights. The parameter K_c is the hardness coefficient, calculated by Equation (46).

$$\mathrm{K}_c = 0.454 + 0.41 \cdot \nu \tag{46}$$

where ν is the Poisson's ratio of the material. The parameter σ_s is calculated by the Equation (47).

$$\sigma_s = \sigma \cdot \sqrt{1 - \frac{3.72 \times 10^{-4}}{\left(N_a \cdot \sigma \cdot \beta_s \right)^2}} \tag{47}$$

where N_a is the number of asperities per unit area.

2.6. Lubricant Properties

The viscosity and density of the lubricant change with temperature and pressure conditions. To consider the influence of these parameters, the modified Higginson and Dowson relationship is used [38,39], as shown in Equations (48) and (49).

$$\rho = (1 - \varrho \cdot (T - T_o)) \cdot \rho_o \cdot \left(1 + \frac{6 \times 10^{-10} (P - P_{atm})}{1 + 1.7 \times 10^{-9} (P - P_{atm})} \right) \tag{48}$$

$$\eta = \eta_o e^{\left[\ln \left(\frac{\eta_o}{\eta_\infty} \right) \cdot \left(\left[1 + \frac{P - P_{atm}}{\varsigma} \right]^Z \left[\frac{T - 138}{T_o - 138} \right]^{-S_o} - 1 \right) \right]} \tag{49}$$

where ϱ is the coefficient of thermal expansion and η_∞ and ς are constants of the model, defined as 6.31×10^{-5} Pas and 1.98×10^8 Pa. The Z and $-S_o$ terms are calculated using Equations (50) and (51).

$$Z = \frac{\varsigma \cdot \alpha_o}{\ln \left(\frac{\eta_o}{\eta_\infty} \right)} \tag{50}$$

$$S_o = \frac{\zeta_o \cdot (T_o - 138)}{\ln \left(\frac{\eta_o}{\eta_\infty} \right)} \tag{51}$$

where ζ_o is the thermo-viscosity coefficient and α_o atmospheric piezo-viscosity, respectively.

3. Numerical Procedure

Figure 2 shows the schematics of the numerical modeling procedure of the model introduced in Section 2. The first step consists of specifying the position parameters (e_o, φ_o), the misalignment parameters (ϕ_x, ϕ_y), and the applied load (W_l). Subsequently, the lubrication film thickness is calculated (see Equation (2)). The solution of the variables $\left(\dot{\varepsilon}_x^{\bar{t}}, \dot{\varepsilon}_y^{\bar{t}} \right)$ is carried out using a Jacobin matrix, the iteration of the Reynolds equation, and the dynamic loads until a dynamic equilibrium is reached. From this information, surface contact conditions (Section 2.5) and surface wear (Section 2.6) are calculated.

Table 1 describes the main parameters and input conditions for the numerical model. The technical characteristics of the engine used as a reference are shown in Table 2.

Table 1. Main input parameters of the numerical model.

Parameters	Symbol	Values
Journal radius	R	30 mm
Bearing length	L	20 mm
Clearance	C	25 μm
Shaft speed	N	2000 rpm
Viscosity	η	0.008 Pa·s

Table 2. Technical characteristics of the engine.

Model	4JJ1
Manufacturer	ISUZU
Cycle	4 strokes
Bore	95.4 mm
Stroke	104.9 mm
Displaced volume	2999 CC
Rated output	95 kW
Injection system	Direct injection
Compression ratio	17.5:1

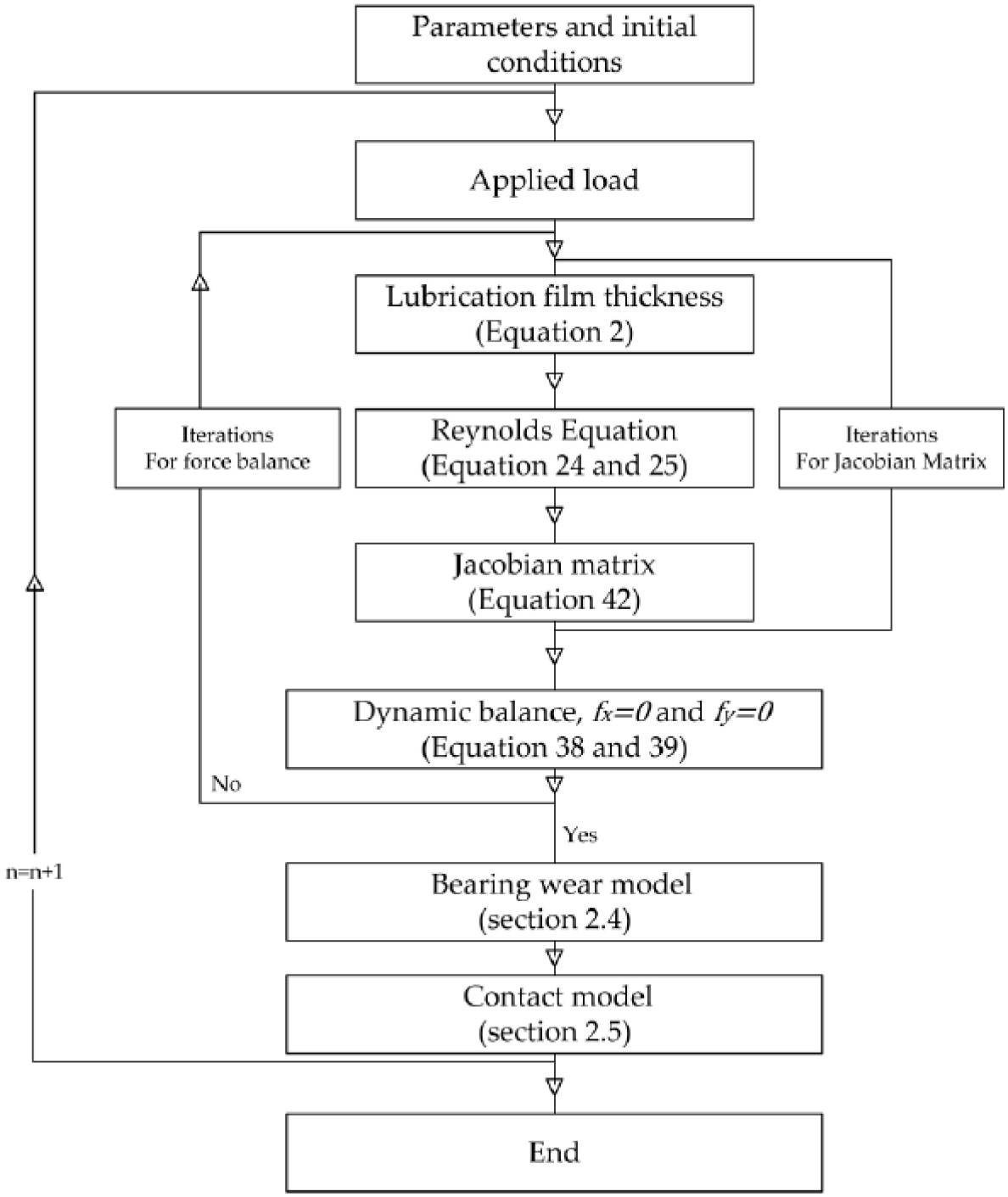

Figure 2. Numerical model diagram.

To validate the reliability of the numerical model, the numerical results are compared with the findings of Ausas et al. [40]. Additionally, a comparison with experimental measurements is made. These measurements consist of capturing the horizontal (X axis) and vertical (Y axis) movement of the bearing. This is done through the use of a triangulation system, using two lasers (model ILD2300LL, Micro-Epsilon, Ortenburg, Germany) located in the horizontal and vertical direction of the bearing. A low pass filter is applied, and an average value of 200 samples is considered. Data acquisition is controlled by software LabView NXG v.4.0. Figure 3 shows the comparison of the estimates of the developed numerical model and the two validation alternatives.

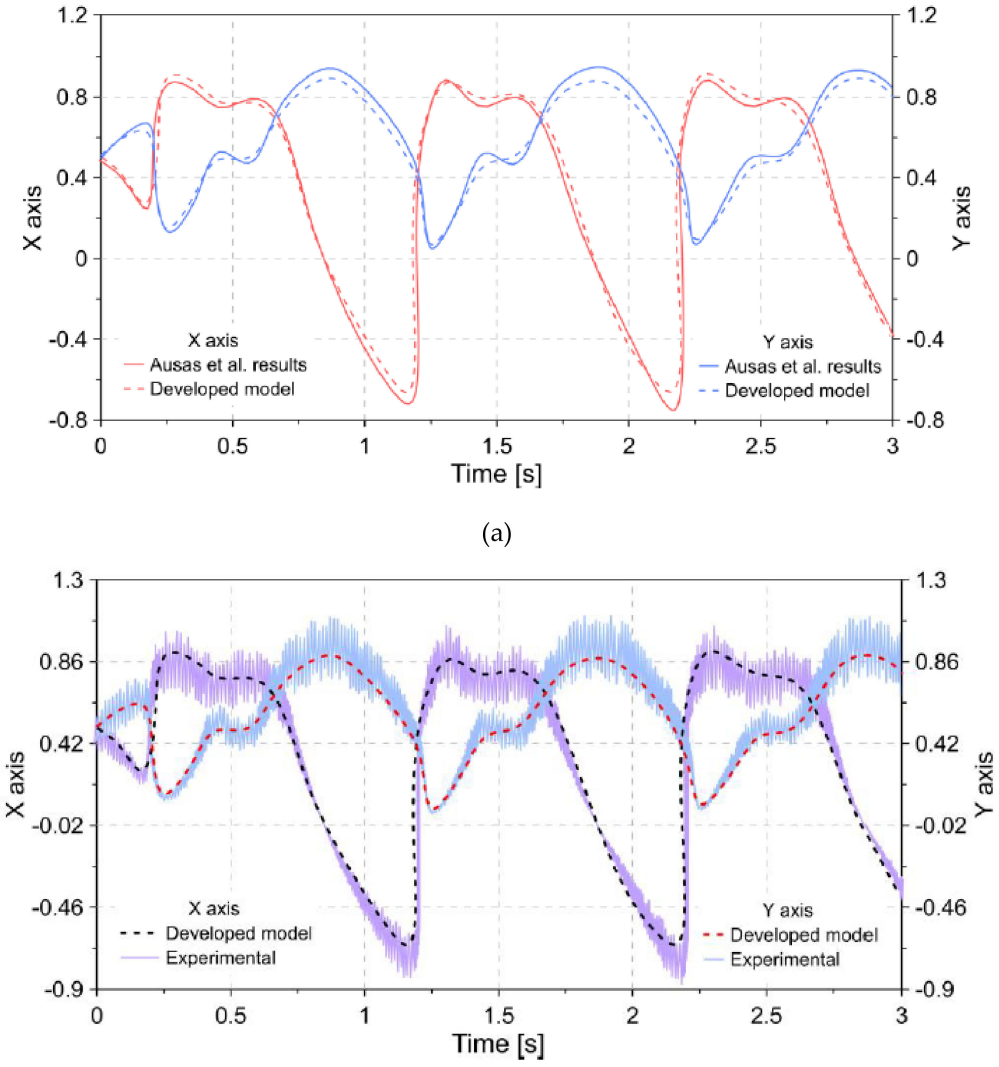

Figure 3. Validation of the numerical model developed using (**a**) the results of Ausas et al. and (**b**) experimental data.

According to the results of Figure 3a, the behavior estimated by the proposed numerical model agrees with the results described by Ausas et al. [40]. In general, the maximum difference between both movements is 11% and 7% for the x- and y-axis, respectively. The relative difference in the validation can be associated with a different time step employed within the simulations. When comparing with the experimental data, a maximum relative error of 20% was observed.

Generally, the average Reynolds equation is used for the hydrodynamic analysis of bearings because it considers the effect of roughness on the behavior of the lubrication film [41]. However, the results shown in Figure 3 indicate that the numerical model used makes it possible to adequately estimate the behavior of the engine bearing. This can be attributed to the fact that the model used considers the effects of cavitation, which also impacts the tribological behavior of the lubricant, allowing an acceptable agreement between the numerical model and the experimental results.

4. Results

4.1. Bearing Journal Movement

Figure 4 describes the movement of the geometric center of the journal for surface roughness of $\sigma = 0.75$ μm, $\sigma = 1$ μm, and $\sigma = 1.25$ μm. The results obtained in Figure 4a show that with a surface roughness of 0.75 μm, there is no contact between the metal surfaces, which

implies that the bearing is protected against wear. Under this condition, the bearing load is supported by the hydrodynamic pressure of the lubricating oil. The minimum dimensionless thickness of the oil film is 0.104, which was obtained at an approximate angle of 295°. With a 33% increase in surface roughness ($\sigma = 1$ µm), an increase in wear was observed during a rotation angle between 210–240°. The maximum dimensionless wear depth is 1.178 and occurs at an angle of 225°. This implies that the surface wear is approximately 18% of the bearing clearance. In the case of surface roughness of ($\sigma = 1.25$ µm), the results show that the maximum depth of wear represents 140% of the bearing clearance.

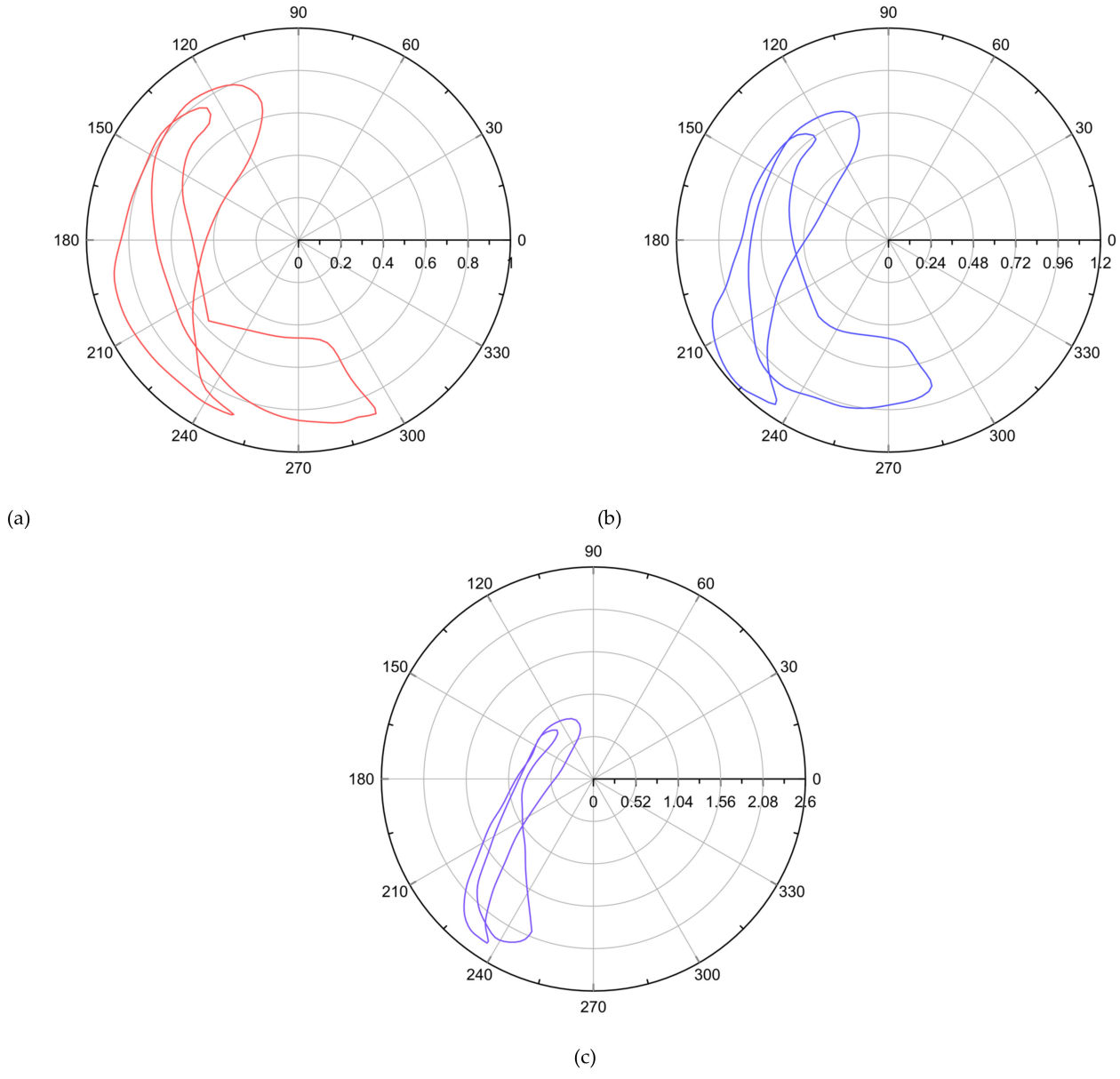

Figure 4. Geometric position of the center of the journal for surface roughness of (**a**) 0.75 µm, (**b**) 1 µm, and (**c**) 1.25 µm.

4.2. Eccentricity Variation

Figure 5 describes the change in the eccentricity ratio according to the load cycle based on different surface roughness conditions. For a roughness condition of $\sigma = 0.75$ µm, it was observed that the eccentricity ratio did not change considerably with time. The maximum eccentricity recorded in this condition was 0.896. However, for roughness greater than 0.75 µm, the results show that the eccentricity ratio is greater than unity ($\varepsilon' > 1$). This is a

consequence of the surface wear produced in the bearing. Additionally, it was observed that the wear process tends to accelerate significantly as roughness increases. In the case of the roughness of $\sigma = 1$ µm, a maximum eccentricity ratio of 0.97, 1.04, and 1.11 was obtained after a time of 12,500, 25,000, and 50,000 s, respectively. For a roughness of $\sigma = 1.25$ µm, the results indicate a maximum eccentricity of 1.24, 1.62, and 2.02, which are obtained in a shorter time (2500, 5000, and 10,000 s, respectively).

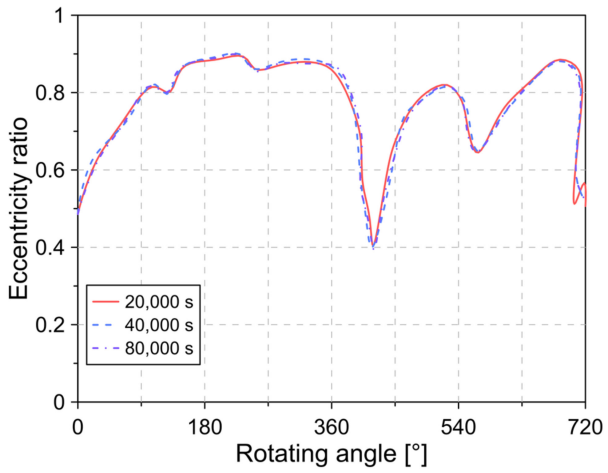

(a)

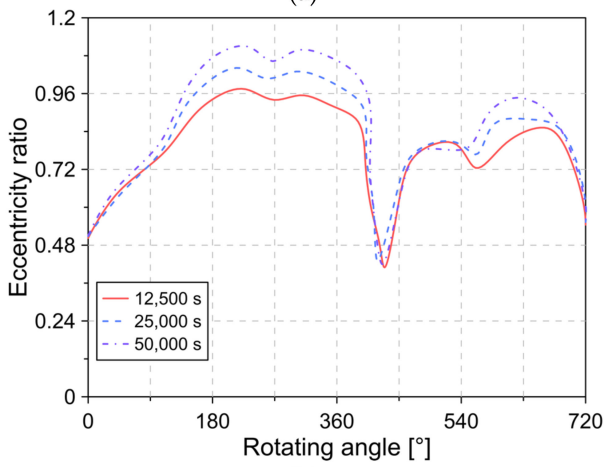

(b)

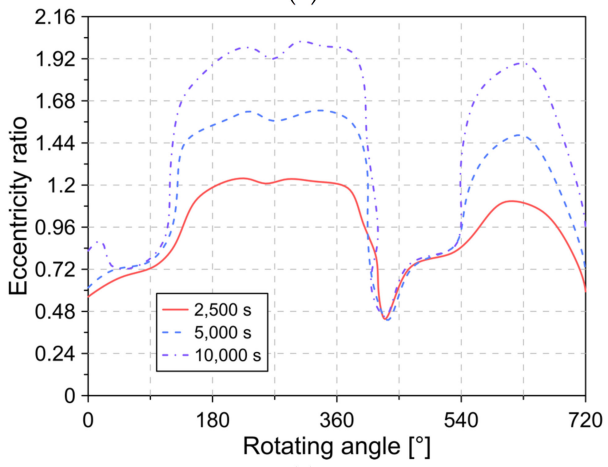

(c)

Figure 5. Changes in the eccentricity ratio for surface roughness of (**a**) 0.75 µm, (**b**) 1 µm, and (**c**) 1.25 µm.

4.3. Wear Rate and Depth

Figure 6 shows the evolution of the wear rate under the different surface roughness conditions. In general, the results show the presence of three or four peaks of wear rate during a rotation angle between 90–720°. In Figure 6a, it was observed that the highest wear rates are located between an angle of 180–360°, which is a consequence of the lower thickness of the lubrication film in this area, as shown in Figure 4a. The three main wear rate peaks in this condition were 0.033, 0.025, and 0.18 µm/s, respectively. For a surface roughness greater than $\sigma = 0.75$ µm, it was observed that the wear rate increased considerably. In the conditions of surface roughness $\sigma = 1$ µm and $\sigma = 1.25$ µm, the results indicate the presence of four peaks of wear rate. The highest rates are 0.874 and 20.016 µm/s for surface roughness of $\sigma = 1$ µm and $\sigma = 1.25$ µm, respectively.

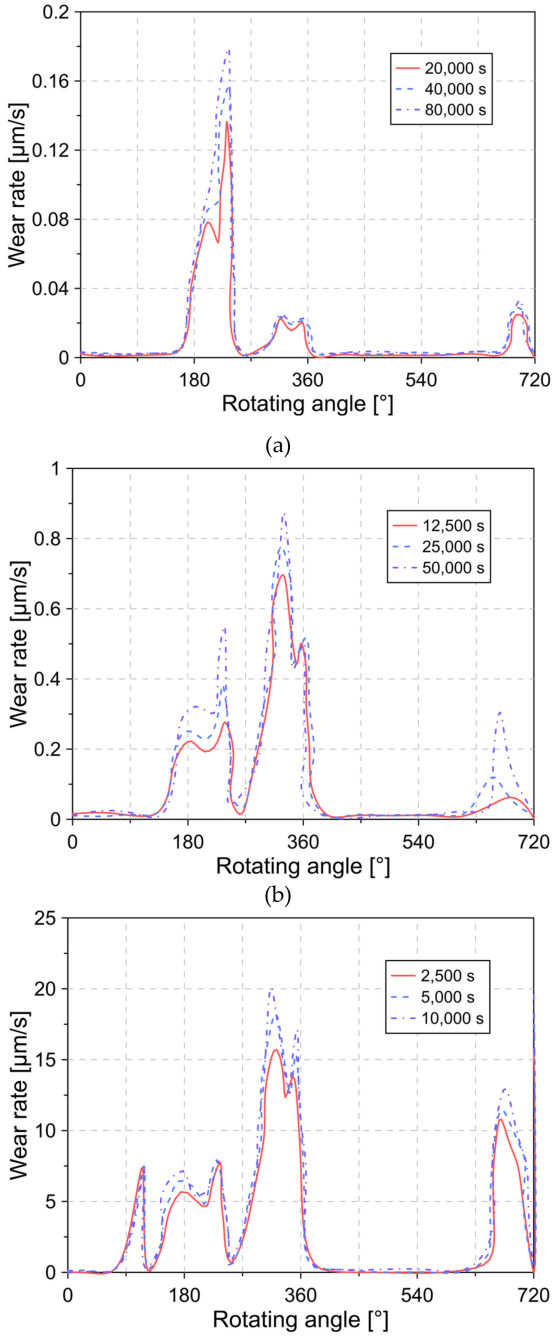

Figure 6. Wear rate for surface roughness of (**a**) 0.75 µm, (**b**) 1 µm, and (**c**) 1.25 µm.

Figure 7 shows the depth of dimensionless wear for different instances of time and surface roughness. The results show that for the roughness of $\sigma = 0.75$ µm, the maximum dimensionless depth of wear is 0.004, 0.006, and 0.007, after a time of 20,000, 40,000, and 80,000 s, respectively. This implies that the depth of wear reaches a maximum of 0.7% of the bearing clearance.

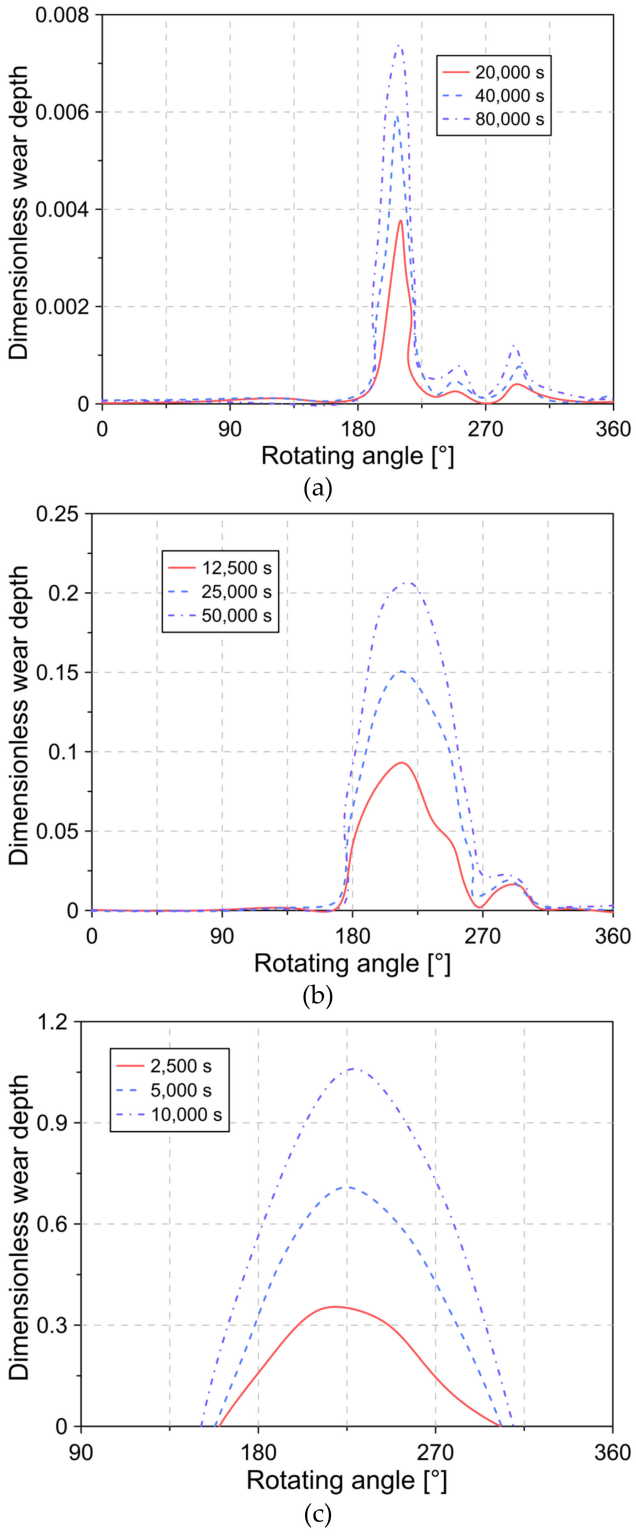

Figure 7. Dimensionless wear depth for a surface roughness of (**a**) 0.75 µm, (**b**) 1 µm, and (**c**) 1.25 µm.

4.4. Movement of Bearing Ends

To evaluate misalignment in engine bearings, two deflection angles (ϕ_x, ϕ_y) must be established, which are two independent parameters that completely define the severity of the misalignment [42]. In this investigation, three different sets of deflection angles are defined, $\{\phi_x = 0.0002,\ \phi_y = -0.0002\}$, $\{\phi_x = 0.0002,\ \phi_y = -0.0004\}$, and $\{\phi_x = -0.0004,\ \phi_y = -0.0004\}$. The surface roughness for all cases is $\sigma = 0.75$ µm. Figure 8 describes the movement of the bearing ends for the different misalignment angles.

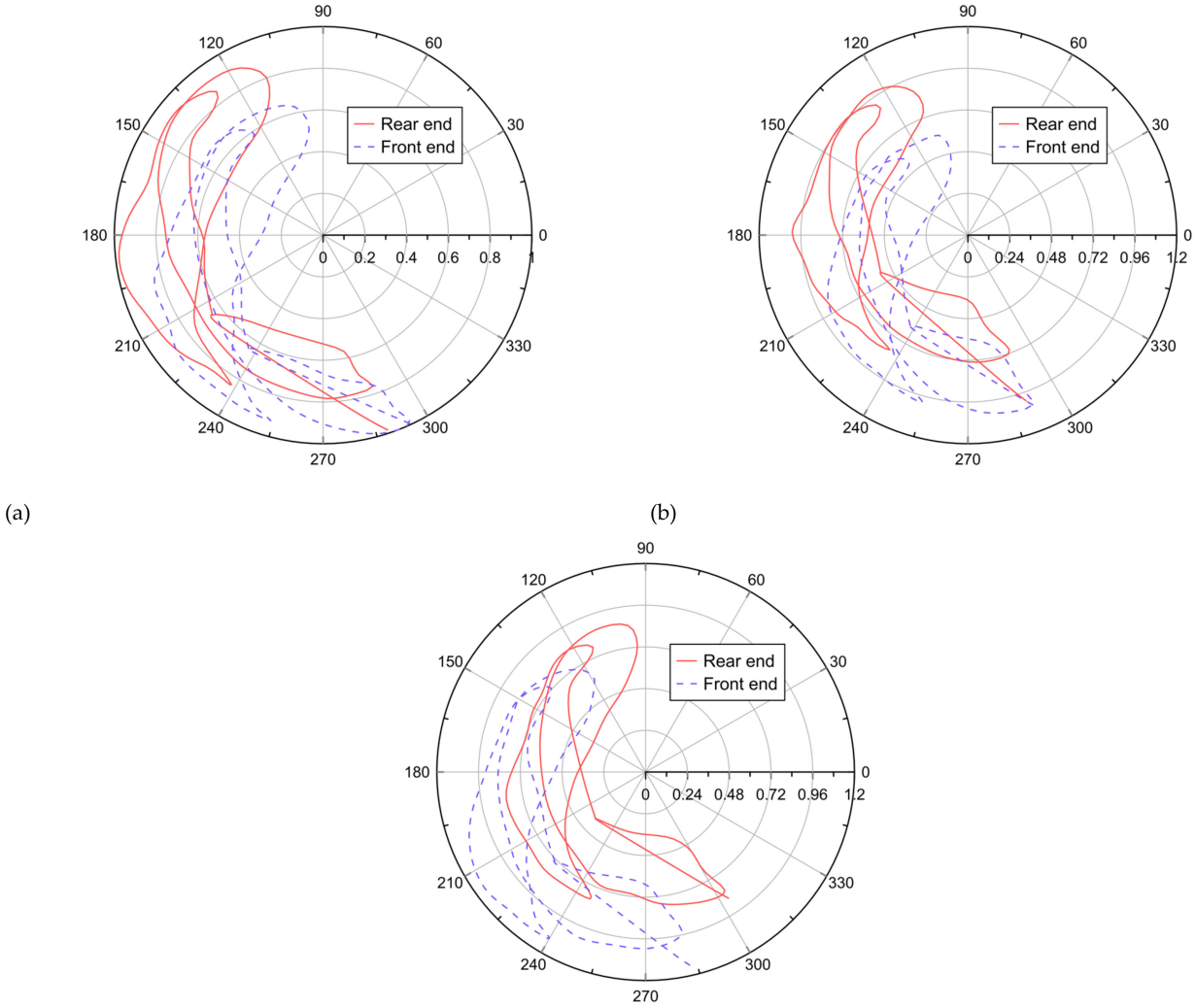

Figure 8. Bearing end movement for (**a**) $\{\phi_x = 0.0002,\ \phi_y = -0.0002\}$, (**b**) $\{\phi_x = 0.0002,\ \phi_y = -0.0004\}$, and (**c**) $\{\phi_x = -0.0004,\ \phi_y = -0.0004\}$.

4.5. Bearing Parameters as a Function of Load

Figure 9 shows the changes in the maximum pressure, friction force, and thickness of the lubrication film that the bearing experiences for a load condition of 50%, 75%, and 100%. The results in Figure 9a show that the maximum hydrodynamic pressure increases with increasing load. However, pressure peaks form at the same time regardless of the applied load percentage. In general, maximum dimensionless pressure of 22.72, 56.93, and 134.24 was observed for a load of 50%, 75%, and 100%, respectively. Similarly, the friction force tends to increase with the highest percentage of the load. In general, a 25% increase in load causes the maximum friction force to increase by 28%. Figure 9c describes the minimum lubrication film thickness for the different loads. The results show that the

dimensionless minimum thickness is 0.54, 0.58, and 0.62 for the load conditions of 100%, 75%, and 50%, respectively.

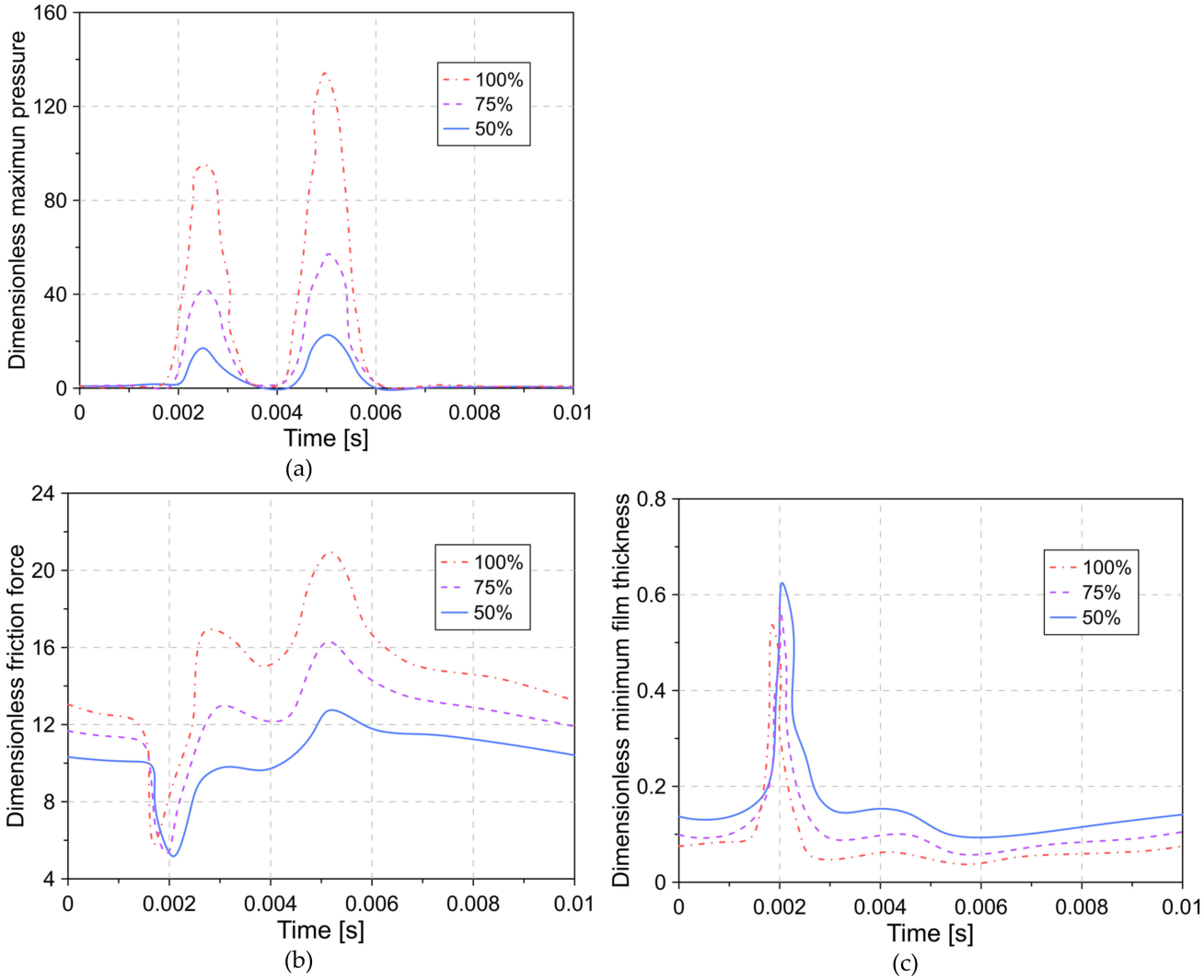

Figure 9. Variation of the bearing parameters, (**a**) maximum pressure, (**b**) friction force, and (**c**) lubrication film thickness.

4.6. Deflection Angle Effect

In Figures 10 and 11, the effect of the angle of deflection ϕ_x and ϕ_y on the moment and the angle of misalignment is described.

The results of Figure 10a show that the positive deflection angle ($\phi_x = 0.0002$) causes a 128% increase in the maximum moment, compared to the negative deflection angle ($\phi_x = -0.0002$). In Figure 10b, it was observed that for an alignment condition ($\phi_x = 0$), the degree of misalignment remains less than 0.24. However, when setting the deflection angles $\phi_x = -0.0002$ and $\phi_x = 0.0002$, the degree of misalignment reaches a maximum of 0.72 and 0.85, respectively.

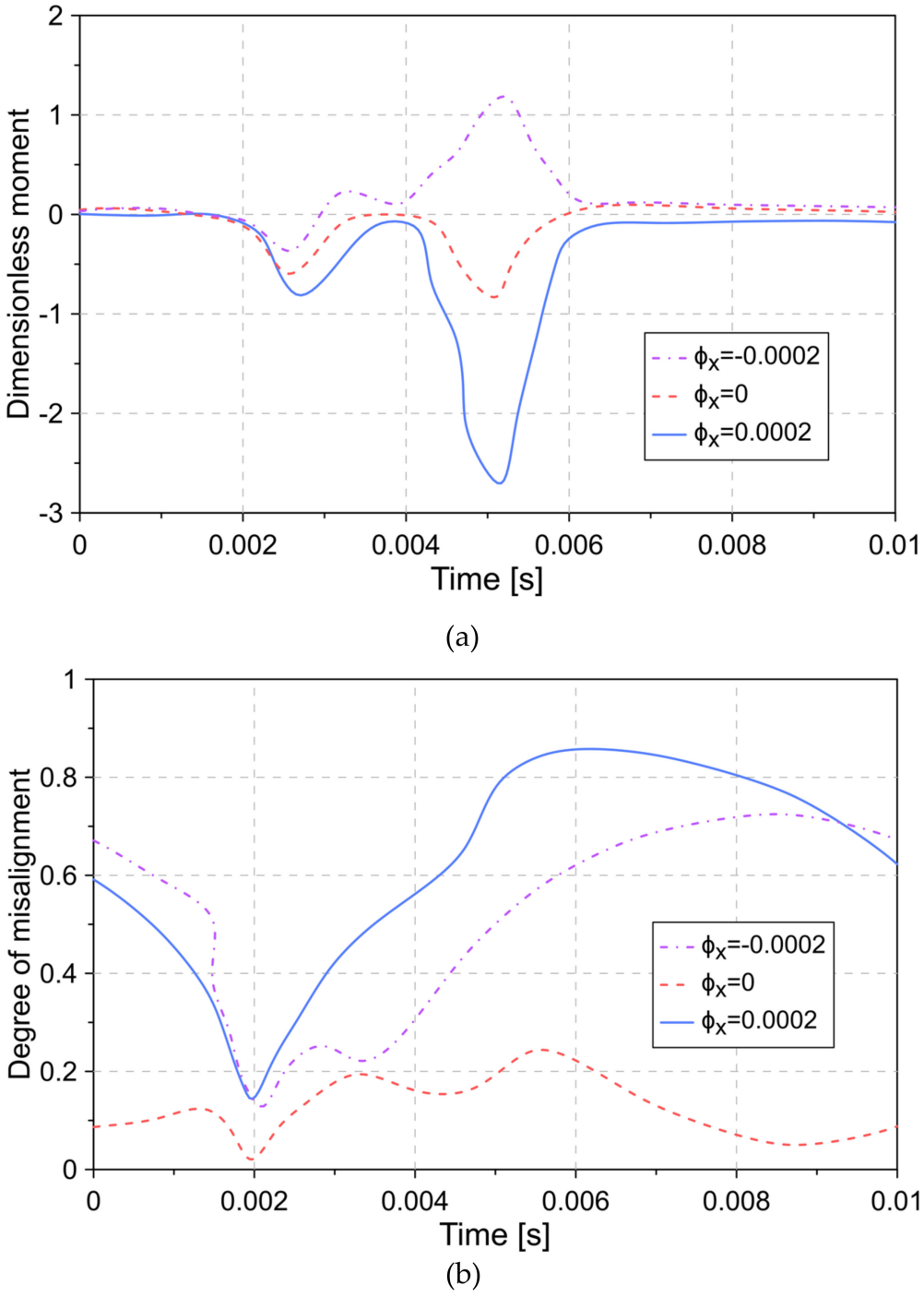

Figure 10. Effect of the angle of deflection ϕ_x on the (**a**) moment and (**b**) angle of misalignment.

In the case of deflection angle ϕ_y (see Figure 11), it was observed that the maximum moment occurs in two peaks. In general, it was observed that the increase in the angle of deflection from $\phi_y = -0.0002$ to $\phi_y = -0.0004$ produces a drastic increase in the maximum moment. The maximum degree of misalignment is 0.95 and 0.24 for a deflection angle of $\phi_y = -0.0004$ and $\phi_y = -0.0002$, respectively.

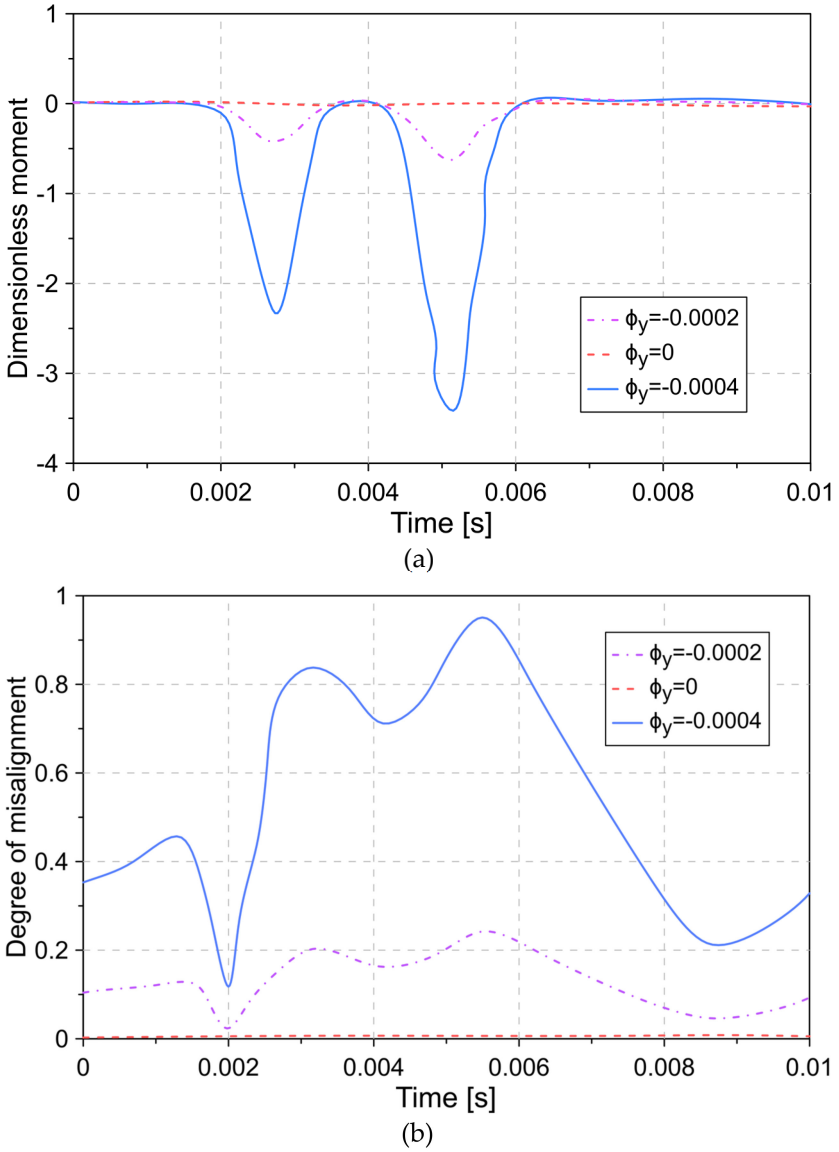

Figure 11. Effect of the angle of deflection ϕ_y on the (**a**) moment and (**b**) angle of misalignment.

5. Discussion

The results in Figure 4 demonstrate that relatively small changes in roughness cause a drastic change in surface wear. In a general sense, it can be stated that higher surface roughness in the bearing fosters surface-to-surface contact, which predominantly leads to catastrophic failures. This pattern is in line with similar investigations [19,32]. Therefore, the importance of surface finishing in bearing design is of relevance to the endurance performance. Moreover, it is worth mentioning that the effect of temperature on the bearing performance is neglected. However, these thermal effects are expected to magnify the load that the bearing experiences, thus increasing the wear damage.

The overall trend of the maximum wear rate agrees with the contact load derived from the eccentricity ratio as they feature a direct relation. In practical applications, the roughness of the bearing surface drops during operation as a result of rubbing the superficial asperities; thus, the wear rate is significantly minimized.

The increase in roughness causes the depth of wear to increase and the time required to reach the maximum depths to decrease abruptly, as shown in Figure 7b,c. For a surface roughness of $\sigma = 1$ μm and $\sigma = 1.25$ μm, a maximum depth of wear equivalent to 21% and 106% of the bearing clearance was obtained, which was reached in a time of 50,000 and

10,000 s, respectively. In all cases, the depth of wear is between a rolling angle of 180 and 270°. Additionally, it was observed that the worn surface tends to a parabolic-like shape.

The results in Figure 8a show that the journal touches the bearing surface at an angle of approximately 293 ° and 188 ° for the front and rear end, respectively. In Figure 8b, it was observed that the increase in the deflection angle (ϕ_y) causes slight wear at both ends. The results show maximum wear of 1.01% and 4.84% for the rear and front end, respectively. By defining a negative deflection angle on both axes $(\phi_x = -0.0004,\ \phi_y = -0.0004)$, it was observed that the rear end of the journal was free of the presence of wear. However, at the front end, there was maximum wear that represented 14% of the bearing clearance.

6. Conclusions

In the present investigation, the influence of wear and misalignment on the bearing performance of a stationary diesel engine subjected to different load conditions (50%, 75%, and 100%) was evaluated. The study consists of the development of a numerical model, which considers the phenomenon of cavitation and the effects of surface roughness through the joint application of the conservation model, and contact pressure model.

In general, the results showed that increasing the surface roughness produces an abrupt rise in bearing wear. For a roughness condition of $\sigma = 1$ μm and $\sigma = 1.25$ μm, the range of radial movement of the journal was greater due to the presence of surface wear, which represented 18% and 140% of the bearing clearance.

The increase in the radial movement of the journal caused an increase in the eccentricity ratio. Additionally, surface roughness led to a drastic increase in the bearing wear rate. The analysis of the different load conditions showed that an increase in this parameter caused an increase in pressure and friction force in the bearing. The latter promoted a reduction in the lubricating oil film. Overall, it was observed that increasing the load by 25% doubled the hydrodynamic pressure. Furthermore, the friction force was increased by 33%, and the lubrication film thickness was reduced by 12%. Moreover, the analysis of the angle of deflections ϕ_x and ϕ_y proved that the moment and the degree of misalignment tended to increase significantly with increasing magnitude of the angle ϕ_y. In the case of angle ϕ_x, the results showed that a negative deflection angle in the x-axis (ϕ_x) magnified the degree of misalignment and the moment. This implies a greater chance of contact with the bearing surface.

In conclusion, the proposed methodology demonstrated to be a feasible and accurate tool to predict and characterize the main parameters that influence the tribological performance of engine bearings. The model featured a concrete limitation on the neglection of the thermal effects that influence the viscosity and other factors such as volumetric expansion that might intensify the wear damage. Therefore, in future studies, there is a pressing need to incorporate the influence of thermal effects in transient conditions to further enhance the numerical model.

Author Contributions: Conceptualization, J.P.R.; methodology, J.P.R., C.P.G., and S.O.A.; software, J.P.R. and C.P.G.; validation, J.P.R., and C.P.G.; formal analysis, J.P.R., C.P.G., and S.O.A.; investigation, J.P.R., C.P.G., and S.O.A.; resources, J.P.R., and S.O.A.; writing—original draft preparation, C.P.G.; writing—review and editing, S.O.A.; funding acquisition, J.P.R., and S.O.A. All authors have read and agreed to the published version of the manuscript.

Funding: This research received no external funding.

Acknowledgments: The authors would like to acknowledge the Universidad Francisco de Paula Santander for their support in the development of this investigation.

Conflicts of Interest: The authors declare no conflict of interest.

Abbreviations

The following abbreviations are used in this manuscript:

Nomenclature

e_o	Eccentricity in the mid-plane of the bearing
e'	Length of the projection of the misaligned journal on the mid-plane
L	Length of the bearing
C	Bearing radial clearance
δ	Depth of wear
A_m	Degree of the misalignment
F_0, F_1, F_2	Viscosity functions
η	Viscosity lubricant
u_s	Shaft speed
$g(\Theta)$	Binary parameter
$\overline{U}$	Dimensionless speed
A_r	Aspect ratio
R	Journal radius
M_j	Mass of the journal
F	Force
M	Moment
$\overline{P}$	Dimensionless hydrodynamic pressure
E'	Hertz elastic modulus
c_k	Wear coefficient
s_d	Sliding distance
H	Hardness
W_l	Load
K_c	Hardness coefficient
N_a	Number of asperities per unit area

Greek Letters

ϕ	Bearing angle
ψ	Misalignment angle
φ_o	Attitude angle between the line of centers and the Y-axis
δ	Depth of wear
ε'	Misalignment eccentricity ratio
β	Bulk modulus of the lubricant
Θ	Fractional film content
ϑ	Wear volume
ρ	Density
Φ	Plasticity index
β_s	Asperity radius
σ_s	Mean of asperity heights
ν	Poisson's ratio
ϱ	Coefficient of thermal expansion
η_∞, ς	Constant model
ζ_o	Thermo-viscosity coefficient
α_o	Atmospheric piezo-viscosity

References

1. Valencia, G.; Duarte, J.; Isaza-Roldan, C. Thermoeconomic Analysis of Different Exhaust Waste-Heat Recovery Systems for Natural Gas Engine Based on ORC. *Appl. Sci.* **2019**, *9*, 4017. [CrossRef]
2. Forero, J.D.; Ochoa, G.V.; Alvarado, W.P. Study of the Piston Secondary Movement on the Tribological Performance of a Single Cylinder Low-Displacement Diesel Engine. *Lubricants* **2020**, *8*, 97. [CrossRef]
3. Forero, J.D.; Ochoa, G.V.; Rojas, J.P. Effect of the Geometric Profile of Top Ring on the Tribological Characteristics of a Low-Displacement Diesel Engine. *Lubricants* **2020**, *8*, 83. [CrossRef]
4. Bergmann, P.; Grün, F.; Summer, F.; Gódor, I. Evaluation of Wear Phenomena of Journal Bearings by Close to Component Testing and Application of a Numerical Wear Assessment. *Lubricants* **2018**, *6*, 65. [CrossRef]
5. Jang, J.Y.; Khonsari, M.M. On the Characteristics of Misaligned Journal Bearings. *Lubricants* **2015**, *3*, 27–53. [CrossRef]

6. Jang, J.; Khonsari, M. Performance and characterization of dynamically-loaded engine bearings with provision for misalignment. *Tribol. Int.* **2019**, *130*, 387–399. [CrossRef]
7. Obregon, L.; Valencia, G.; Forero, J.D. Efficiency Optimization Study of a Centrifugal Pump for Industrial Dredging Applications Using CFD. *Int. Rev. Model. Simul.* **2019**, *12*, 245. [CrossRef]
8. Orozco, T.; Herrera, M.; Forero, J.D. CFD Study of Heat Exchangers Applied in Brayton Cycles: A Case Study in Supercritical Condition Using Carbon Dioxide as Working Fluid. *Int. Rev. Model. Simul.* **2019**, *12*, 72–82. [CrossRef]
9. Orozco, W.; Acuña, N.; Forero, J.D. Characterization of Emissions in Low Displacement Diesel Engines Using Biodiesel and Energy Recovery System. *Int. Rev. Mech. Eng.* **2017**, *13*, 420. [CrossRef]
10. Chasalevris, A.; Dohnal, F.; Chatzisavvas, I. Experimental detection of additional harmonics due to wear in journal bearings using excitation from a magnetic bearing. *Tribol. Int.* **2014**, *71*, 158–167. [CrossRef]
11. Beheshti, A.; Khonsari, M. An engineering approach for the prediction of wear in mixed lubricated contacts. *Wear* **2013**, *308*, 121–131. [CrossRef]
12. De La Hoz, J.S.; Valencia, G.; Forero, J.D. Reynolds Averaged Navier–Stokes Simulations of the Airflow in a Centrifugal Fan Using OpenFOAM. *Int. Rev. Model. Simul.* **2019**, *12*, 230. [CrossRef]
13. Ochoa, G.V.; Isaza-Roldan, C.; Forero, J.D. Economic and Exergo-Advance Analysis of a Waste Heat Recovery System Based on Regenerative Organic Rankine Cycle under Organic Fluids with Low Global Warming Potential. *Energies* **2020**, *13*, 1317. [CrossRef]
14. Consuegra, F.; Bula, A.; Guillín, W.; Sánchez, J.; Forero, J.D. Instantaneous in-Cylinder Volume Considering Deformation and Clearance due to Lubricating Film in Reciprocating Internal Combustion Engines. *Energies* **2019**, *12*, 1437. [CrossRef]
15. Diaz, G.A.; Forero, J.D.; Garcia, J.; Rincon, A.; Fontalvo, A.; Bula, A.J.; Padilla, R.V. Maximum Power From Fluid Flow by Applying the First and Second Laws of Thermodynamics. *J. Energy Resour. Technol.* **2017**, *139*, 032903. [CrossRef]
16. Nabhan, A.; Rashed, A.; Ghazaly, N.M.; Abdo, J.; Haneef, M.D. Tribological Properties of Al_2O_3 Nanoparticles as Lithium Grease Additives. *Lubricants* **2021**, *9*, 9. [CrossRef]
17. Aghdam, A.; Khonsari, M. Prediction of wear in grease-lubricated oscillatory journal bearings via energy-based approach. *Wear* **2014**, *318*, 188–201. [CrossRef]
18. Chun, S.M.; Khonsari, M.M. Wear simulation for the journal bearings operating under aligned shaft and steady load during start-up and coast-down conditions. *Tribol. Int.* **2016**, *97*, 440–466. [CrossRef]
19. Sander, D.E.; Allmaier, H.; Priebsch, H.; Reich, F.; Witt, M.; Skiadas, A.; Knaus, O. Edge loading and running-in wear in dynamically loaded journal bearings. *Tribol. Int.* **2015**, *92*, 395–403. [CrossRef]
20. Jia, H.; Li, J.; Wang, J.; Xiang, G.; Xiao, K.; Han, Y. Micropitting Fatigue Wear Simulation in Conformal-Contact Under Mixed Elastohydrodynamic Lubrication. *J. Tribol.* **2019**, *141*, 061501-27. [CrossRef]
21. Gu, C.; Meng, X.; Wang, S.; Ding, X. Modeling a Hydrodynamic Bearing With Provision for Misalignments and Textures. *J. Tribol.* **2019**, *142*, 1–29. [CrossRef]
22. Li, L.; Zhang, D.; Xie, Y. Effect of misalignment on the dynamic characteristic of MEMS gas bearing considering rarefaction effect. *Tribol. Int.* **2019**, *139*, 22–35. [CrossRef]
23. Li, B.; Sun, J.; Zhu, S.; Fu, Y.; Zhao, X.; Wang, H.; Teng, Q.; Ren, Y.; Li, Y.; Zhu, G. Thermohydrodynamic lubrication analysis of misaligned journal bearing considering the axial movement of journal. *Tribol. Int.* **2019**, *135*, 397–407. [CrossRef]
24. Zhu, S.; Sun, J.; Li, B.; Zhu, G. Thermal turbulent lubrication analysis of rough surface journal bearing with journal misalignment. *Tribol. Int.* **2020**, *144*, 106109. [CrossRef]
25. Feng, H.; Jiang, S.; Ji, A. Investigations of the static and dynamic characteristics of water-lubricated hydrodynamic journal bearing considering turbulent, thermohydrodynamic and misaligned effects. *Tribol. Int.* **2019**, *130*, 245–260. [CrossRef]
26. Zheng, L.; Zhu, H.; Zhu, J.; Deng, Y. Effects of oil film thickness and viscosity on the performance of misaligned journal bearings with couple stress lubricants. *Tribol. Int.* **2020**, *146*, 106229. [CrossRef]
27. Xie, Z.; Song, P.; Hao, L.; Shen, N.; Zhu, W.; Liu, H.; Shi, J.; Wang, Y.; Tian, W. Investigation on effects of Fluid-Structure-Interaction (FSI) on the lubrication performances of water lubricated bearing in primary circuit loop system of nuclear power plant. *Ann. Nucl. Energy* **2020**, *141*, 107355. [CrossRef]
28. Ochoa, G.V.; Isaza-Roldan, C.; Forero, J.D. A phenomenological base semi-physical thermodynamic model for the cylin-der and exhaust manifold of a natural gas 2-megawatt four-stroke internal combustion engine. *Heliyon* **2019**, *5*, e02700. [CrossRef]
29. Ochoa, G.V.; Peñaloza, C.A.; Forero, J.D. Thermoeconomic Optimization with PSO Algorithm of Waste Heat Recovery Systems Based on Organic Rankine Cycle System for a Natural Gas Engine. *Energies* **2019**, *12*, 4165. [CrossRef]
30. Xie, Z.; Rao, Z.; Liu, H. Effect of Surface Topography and Structural Parameters on the Lubrication Performance of a Water-Lubricated Bearing: Theoretical and Experimental Study. *Coatings* **2019**, *9*, 23. [CrossRef]
31. Xie, Z.; Rao, Z.-S.; Ta, N.; Liu, L. Investigations on transitions of lubrication states for water lubricated bearing. Part I: Determination of friction coefficients and film thickness ratios. *Ind. Lubr. Tribol.* **2016**, *68*, 404–415. [CrossRef]
32. Xie, Z.; Rao, Z.-S.; Ta, N.; Liu, L. Investigations on transitions of lubrication states for water lubricated bearing. Part II: Further insight into the film thickness ratio lambda. *Ind. Lubr. Tribol.* **2016**, *68*, 416–429. [CrossRef]
33. Jang, J.Y.; Khonsari, M.M. On the Behavior of Misaligned Journal Bearings Based on Mass-Conservative Thermohydrodynamic Analysis. *J. Tribol.* **2009**, *132*, 011702. [CrossRef]

34. Vijayaraghavan, D.; Keith, T. Effect of cavitation on the performance of a grooved misaligned journal bearing. *Wear* **1989**, *134*, 377–397. [CrossRef]
35. Elrod, H.G.; Adams, M.L. A computer program for cavitation and starvation problems. *Cavitation Relat. Phenom. Lubricants* **1975**, 37–41.
36. Archard, J.F. Contact and Rubbing of Flat Surfaces. *J. Appl. Phys.* **1953**, *24*, 981–988. [CrossRef]
37. Kogut, L.; Etsion, I. A Finite Element Based Elastic-Plastic Model for the Contact of Rough Surfaces. *Tribol. Trans.* **2003**, *46*, 383–390. [CrossRef]
38. Dowson, D.; Higginson, G.R. A Numerical Solution to the Elasto-Hydrodynamic Problem. *J. Mech. Eng. Sci.* **1959**, *1*, 6–15. [CrossRef]
39. Yang, P.; Cui, J.; Jin, Z.M.; Dowson, D. Transient elastohydrodynamic analysis of elliptical contacts. Part 2: Thermal and Newtonian lubricant solution. *Proc. Inst. Mech. Eng. Part J J. Eng. Tribol.* **2005**, *219*, 187–200. [CrossRef]
40. Ausas, R.F.; Jai, M.; Buscaglia, G.C. A Mass-Conserving Algorithm for Dynamical Lubrication Problems With Cavitation. *J. Tribol.* **2009**, *131*, 031702. [CrossRef]
41. Zhang, H.; Hua, M.; Dong, G.-N.; Zhang, D.-Y.; Chin, K.-S. A mixed lubrication model for studying tribological behaviors of surface texturing. *Tribol. Int.* **2016**, *93*, 583–592. [CrossRef]
42. Paranjpe, R.S. A Study of Dynamically Loaded Engine Bearings Using a Transient Thermohydrodynamic Analysis. *Tribol. Trans.* **1996**, *39*, 636–644. [CrossRef]